Article

A Generic Matrix Method to Model the Magnetics of Multi-Coil Air-Cored IPT Systems †

Prasanth Venugopal *†, Soumya Bandyopadhyay, Pavol Bauer and Jan Abraham Ferreira

Delft University of Technology (TU Delft), Mekelweg 04, 2628 CD, Delft, The Netherlands;
s.bandyopadhyay-1@tudelft.nl (S.B.); p.bauer@tudelft.nl (P.B.); j.a.ferreira@tudelft.nl (J.A.F.)

* Correspondence: v.prasanth@tudelft.nl; Tel.: +31(0)15 2786016

† This paper is an extended publication of conference papers published by authors in [1]-[2]

Abstract: This paper deals with a generic methodology to evaluate the magnetic parameters of contactless power transfer systems. Neumann's integral has been used to create a matrix method that can model the magnetics of single coils (circle, square, rectangle). The principle of superposition has been utilised to extend the theory to multi-coil geometries such as double circular, double rectangle and double rectangle quadrature assuming linearity of magnetics. Numerical and experimental validation has been performed to validate the analytical models developed. A rigorous application of the analysis has been carried out to study misalignment and hence the efficacy of various geometries to misalignment tolerance. Comparison of single-coil and multi-coil shapes considering coupling variation with misalignment, power transferred and maximum efficiency is carried out.

Keywords: air-cored; contactless; coupling; inductive power transfer; magnetics; matrix; modelling; multi-coil

1. Introduction

Inductive Power Transfer (IPT) relies on electromagnetic fields to transfer energy between circuits that are not physically connected. Loosely coupled coils that are used in IPT systems suffer from high leakage fields that demand reactive power, constricting large power transfer at high efficiency. To nullify this effect, capacitive compensation is carried out such that reactive power exchange take places between the capacitors and inductors with the source directly connected to the load, improving power factor, power transfer and efficiency.

Inductive Power Transfer systems due to its non-contact nature allows efficient power flow to happen with reduced maintenance, is safe, clean and reliable. Thus, applications spanning from low power medical devices (mW) to mining (MW) have been found in literature [3]. Other applications include consumer electronics, EVs, underwater power delivery etc [4], [5]. A number of resonant topologies have been proposed and several coil shapes and designs have been researched in this field [3]. However, an analytical framework that studies the impact of coil shape and misalignment in IPT systems in a rigorous manner is found missing.

The magnetic design and its optimization is an important step in the design of IPT systems. Typically, coil optimization and magnetic parameter estimation (L_1, L_2, M, k) are performed relying on EM field solvers and/or combing with evolutionary algorithms [6,7]. In other work, numerical techniques (solving look-up tables (book of Grover [8]), solving Bessel functions [9], solving elliptical integrals [10]) and PEEC solvers [11,12] are used to achieve the same. In Grover's book, there is available closed-form expressions for self-inductance of a number of polygonal shapes. However, all the equations are developed for single-turns ignoring the effect of the air-gap between turns resulting in a reduction in a reduced fill factor.

In this paper, we bridge this gap by taking into account the effect of turns (increase in perimeter for every new turn) as well as any incipient air-gap by using a matrix manipulation. This extends to both single and multi coil geometries and their magnetic behaviour is analysed.

2. Neumann's Integral

The mutual inductance between two current carrying circuits assuming uniform cross-sectional current density and neglecting radiation can be written in terms of the differential length vector of the two circuits $d\vec{l}_1$, $d\vec{l}_2$ separated by a distance r_{12} as

$$L_{12} = \frac{\lambda_2}{i_1} = \frac{\mu_0}{4\pi} \oint_{c_1} \oint_{c_2} \frac{d\vec{l}_1 . d\vec{l}_2}{r_{12}} \tag{1}$$

In equation 1, contours c_1 and c_2 are along the middle edge of the circuits 1 and 2 (primary and secondary) respectively. This equation is generic, order independent and can be adapted to model self-inductance by considering the contours c_1 and c_2 as along the middle edge of the conductor and the inner edge of the wire.

2.1. Circular Coils

In case of a pair of circular coils, the application of Neumann's integral as in (1), the two contours c_1 and c_2 represent the contour of current filaments assumed to be in the middle of primary and secondary. Now, consider the case of a misaligned circular coil pair, composed of wires of circular cross-section of radius r and with an air-gap l_g between turns. Such a coil pair is indicated in Figure 1. The inner radius of the i^{th} turn of the primary and j^{th} turn of secondary are $R_i = R_p + (i-1)(2r +$

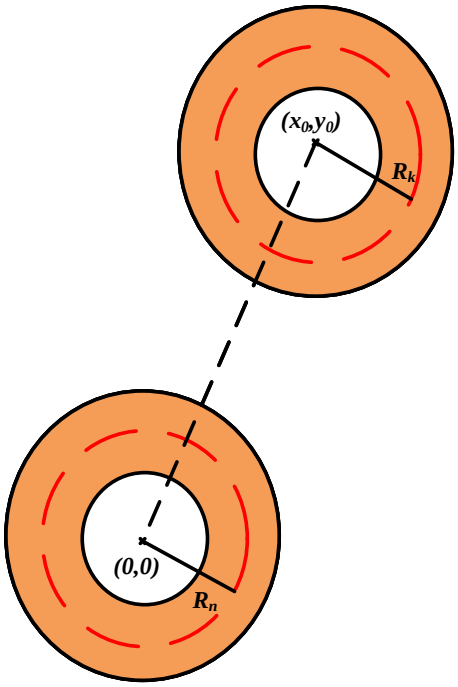

Figure 1. A coupled circular coil system with primary having $i = 1, 2..., n$ turns and the secondary having $j = 1, 2..., k$ turns, the radii of the mid current contour of the n^{th} primary turn and k^{th} secondary turn are R_n and R_k.

$l_g)$, $R_j = R_s + (j-1)(2r + l_g)$ respectively. In such a case, the partial mutual inductance is written in terms of azimuths, ϕ_i and ϕ_j of the respective coils as

$$M_{ij} = \frac{\mu_0}{4\pi} \times \left[\int_{\phi_i=0}^{2\pi} \int_{\phi_j=0}^{2\pi} I d\phi_i d\phi_j \right] \tag{2}$$

Preprints (www.preprints.org) | NOT PEER-REVIEWED | Posted: 26 May 2017 doi:10.20944/preprints201705.0191.v1

Peer-reviewed version available at Energies 2017, 10, , 774; doi:10.3390/en10060774

Where I, R_i, R_j are defined as

$$I = \frac{R_i R_j \sin\phi_i \sin\phi_j + R_i R_j \cos\phi_i \cos\phi_j}{\sqrt{\left(R_i \cos\phi_i - (x_0 + R_j \cos\phi_j)\right)^2 + \left(R_i \sin\phi_i - (y_0 + R_j \sin\phi_j)\right)^2}} \tag{3}$$

The final mutual inductance can be defined for primary having $'n'$ turns and secondary with $'k'$ turns as

$$M = \sum_{i=1}^{n} \sum_{j=1}^{k} M_{ij} \tag{4}$$

The self-inductances can be extracted similarly from (4) by defining the radius of the middle edge and the inner edge of each turn.

2.2. Rectangular Coils

A single turn rectangular coil is shown in Figure 2. A rectangular structure can be split into four sections ($l_{1'}, l_{2'}, ..l_{4'}$), each of which refer to conductors in the top, bottom, left and right respectively In such a case, (1) can be written in terms of the various sections of the coil as

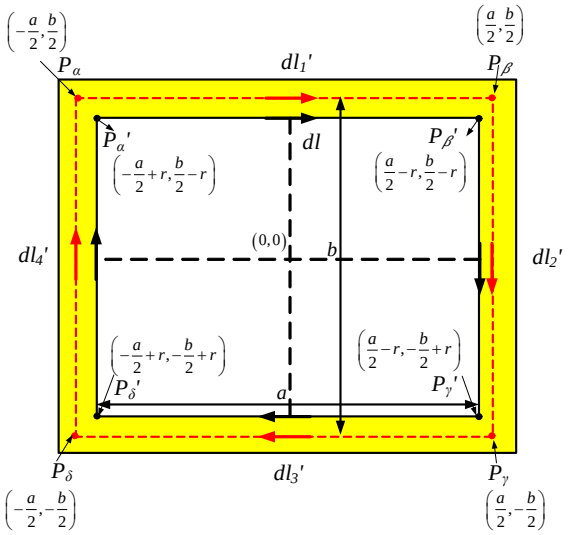

Figure 2. Definition of the contour of the elementary inner edge of a single turn rectangular coil dl and the various sections of the contour of the elementary line along the centre of the wire $(dl_{1'}, dl_{2'}, ..dl_{4'})$. For further evaluation, the contour of dl can be split at the top, right, bottom and left sections as $(dl_1, dl_2, ..dl_4)$.

$$L = \frac{\mu_0}{4\pi} \times \left[\oint_{l_{1'}} \oint_{l_1} \frac{d\vec{\mathbf{l}}_{\mathbf{1'}} . d\vec{\mathbf{l}}_{\mathbf{1}}}{r_{1'1}} + \oint_{l_{2'}} \oint_{l_1} \frac{d\vec{\mathbf{l}}_{\mathbf{2'}} . d\vec{\mathbf{l}}_{\mathbf{1}}}{r_{2'1}} + \oint_{l_{3'}} \oint_{l_1} \frac{d\vec{\mathbf{l}}_{\mathbf{3'}} . d\vec{\mathbf{l}}_{\mathbf{1}}}{r_{3'1}} + \oint_{l_{4'}} \oint_{l_1} \frac{d\vec{\mathbf{l}}_{\mathbf{4'}} . d\vec{\mathbf{l}}_{\mathbf{1}}}{r_{4'1}} \right] \tag{5}$$

This can be written as a matrix in the form where the rows represent the section of the conductor that carriers the current (section of the contour of the centre) and columns represent the section on

which the inductance contribution is considered. Each element of the matrix is a partial inductance (self partial inductance $(i = j)$ and mutual partial inductance $(i \neq j)$).

$$L_{ij} = \frac{\mu_0}{4\pi} \times \begin{bmatrix} \oint_{l_{1'}} \oint_{l_1} \frac{d\vec{l}_{1'}.d\vec{l}_1}{r_{1'1}} & \oint_{l_{1'}} \oint_{l_2} \frac{d\vec{l}_{1'}.d\vec{l}_2}{r_{1'2}} & \cdots & \oint_{l_{1'}} \oint_{l_4} \frac{d\vec{l}_{1'}.d\vec{l}_4}{r_{1'4}} \\ \oint_{l_{2'}} \oint_{l_1} \frac{d\vec{l}_{2'}.d\vec{l}_1}{r_{2'1}} & \oint_{l_{2'}} \oint_{l_2} \frac{d\vec{l}_{2'}.d\vec{l}_2}{r_{2'2}} & \cdots & \oint_{l_{2'}} \oint_{l_4} \frac{d\vec{l}_{2'}.d\vec{l}_4}{r_{2'4}} \\ \oint_{l_{3'}} \oint_{l_1} \frac{d\vec{l}_{3'}.d\vec{l}_1}{r_{3'1}} & \oint_{l_{3'}} \oint_{l_2} \frac{d\vec{l}_{3'}.d\vec{l}_2}{r_{3'2}} & \cdots & \oint_{l_{3'}} \oint_{l_4} \frac{d\vec{l}_{3'}.d\vec{l}_4}{r_{3'4}} \\ \oint_{l_{4'}} \oint_{l_1} \frac{d\vec{l}_{4'}.d\vec{l}_1}{r_{4'1}} & \oint_{l_{4'}} \oint_{l_2} \frac{d\vec{l}_{4'}.d\vec{l}_2}{r_{4'2}} & \cdots & \oint_{l_{4'}} \oint_{l_4} \frac{d\vec{l}_{4'}.d\vec{l}_4}{r_{4'4}} \end{bmatrix} \tag{6}$$

Self-inductance of this rectangular coil can be written as

$$L = \sum_{i=1}^{4} \sum_{j=1}^{4} L_{ij} \tag{7}$$

Since the orthogonal terms in the vector dot product reduces to a zero. For eg: $(d\vec{l}_{1'}.d\vec{l}_2 = dx_1\hat{i}.dy\hat{j} = 0)$.

$$L = \begin{bmatrix} L_{11} & 0 & L_{13} & 0 \\ 0 & L_{22} & 0 & L_{24} \\ L_{31} & 0 & L_{33} & 0 \\ 0 & L_{42} & 0 & L_{44} \end{bmatrix} \tag{8}$$

Thus, the total external self-inductance can be written in terms of $L_a = L_{11} = L_{33}$, $L_b = L_{22} = L_{44}$, $M_a = L_{13} = L_{31}$, $M_b = L_{24} = L_{42}$ as

$$L = 2(L_a + L_b - M_a - M_b) \tag{9}$$

Where, the self-partial inductances $(L_a, L_b = L_{(a=b)})$ are given by

$$\begin{aligned} L_a &= \frac{\mu_0}{4\pi} \times \left[\int_{-\frac{a}{2}+r}^{\frac{a}{2}-r} dx_1 \int_{-\frac{a}{2}}^{\frac{a}{2}} \frac{dx_2}{\sqrt{(x_2 - x_1)^2 + r^2}} \right] \\ L_a &= (a-r) \ln \left| \frac{a - r + \sqrt{r^2 + (a-r)^2}}{-a + r + \sqrt{r^2 + (-a+r)^2}} \right| + r \ln \left| \frac{-r + \sqrt{2}r}{r + \sqrt{2}r} \right| \\ &\quad + 2\sqrt{2}r - \sqrt{(r^2 + (a-r)^2)} - \sqrt{(r^2 + (-a+r)^2)} \end{aligned} \tag{10}$$

Also, the mutual partial inductances $(M_a, M_b = M_{(a \leftrightarrow b)})$ are given as

$$M_a = \frac{\mu_0}{4\pi} \times \left[\int_{-\frac{a}{2}+r}^{\frac{a}{2}-r} dx_3 \int_{-\frac{a}{2}}^{\frac{a}{2}} \frac{dx_2}{\sqrt{(x_2 - x_3)^2 + (b-r)^2}} \right] \tag{11}$$

3. Multi-Turn Charge Pads

A multi-turn coil is shown in Figure 3. Consider the per-turn inductance written as L_{ijlk} which represents the partial inductance contribution due to current flowing through i^{th} turn, j^{th} section on the l^{th} turn, k^{th} section. In such a case, it is important to derive the expressions of the mutual partial inductances considering that the dimensions of the coil change with corresponding change in number

of turns. It is useful to list the vertices of the extremes of the contour along the center of the wire as well as along the inner edge of the wire for the N^{th} winding.

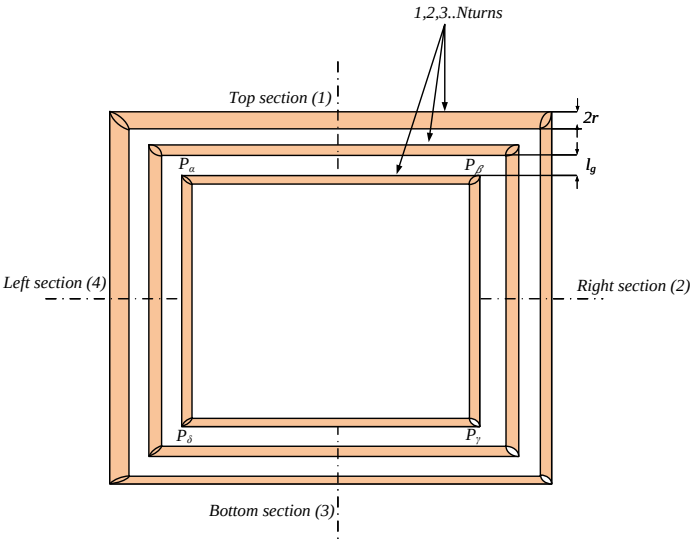

Figure 3. A multi turn inductor with dimensions defined from the centre of a wire of circular section with radius r and wound in a manner such that air gap is uniform (l_g) and the center contour of the wire has vertices $P_\alpha = (-a/2, b/2)$, $P_\beta = (a/2, b/2)$, $P_\gamma = (a/2, -b/2)$, $P_\delta = (-a/2, -b/2)$. The N^{th} turn 'α' vertex has its middle edge and inner edge with vertices $P_{N\alpha} = \left[-\frac{a}{2} - (N-1)(2r + l_g), \frac{b}{2} + (N-1)(2r + l_g)\right]$ and $P_{N\alpha i} = \left[\left(-\frac{a}{2} + r\right) - (N-1)(2r + l_g), \left(\frac{b}{2} - r\right) + (N-1)(2r + l_g)\right]$.

The partial self-inductance of the N^{th} turn (due to the 1^{st} section) can be derived as

$$L_{N1N1} = \frac{\mu_0}{4\pi} \times \left[\int_{k_1}^{k_2} dx_1 \int_{\alpha}^{\beta} \frac{dx_2}{\sqrt{(x_2 - x_1)^2 + r^2}}\right] \tag{12}$$

Where,

$$\begin{aligned} k_1 = \left(-\frac{a}{2} + r\right) - (N-1)(2r + l_g), k_2 = \left(\frac{a}{2} - r\right) + (N-1)(2r + l_g) \\ \alpha = -\frac{a}{2} - (N-1)(2r + l_g), \beta = \frac{a}{2} + (N-1)(2r + l_g) \end{aligned} \tag{13}$$

The result of such an integration is

$$\frac{\mu_0}{4\pi} \times [I(C = \beta) - I(C = \alpha)] \tag{14}$$

Where,

$$I(C) = \sqrt{r^2 + (C - k_2)^2} - \sqrt{r^2 + (C - k_1)^2} + \ln \left| \frac{\left(\sqrt{r^2 + (C - k_1)^2} + (C - k_1)\right)^{(C - k_1)}}{\left(\sqrt{r^2 + (C - k_2)^2} + (C - k_2)\right)^{(C - k_2)}} \right| \tag{15}$$

The self-inductance matrix can be written as

Preprints (www.preprints.org) | NOT PEER-REVIEWED | Posted: 26 May 2017 doi:10.20944/preprints201705.0191.v1

Peer-reviewed version available at Energies 2017, 10, , 774; doi:10.3390/en10060774

$$L_{ijlk} = \frac{\mu_0}{4\pi} \times \begin{bmatrix} \sum_{i=1}^{N}\sum_{l=1}^{N} L_{i1l1} & 0 & -\sum_{i=1}^{N}\sum_{l=1}^{N} L_{i1l3} & 0 \\ 0 & \sum_{i=1}^{N}\sum_{l=1}^{N} L_{i2l2} & 0 & -\sum_{i=1}^{N}\sum_{l=1}^{N} L_{i2l4} \\ -\sum_{i=1}^{N}\sum_{l=1}^{N} L_{i3l1} & 0 & \sum_{i=1}^{N}\sum_{l=1}^{N} L_{i3l3} & 0 \\ 0 & -\sum_{i=1}^{N}\sum_{l=1}^{N} L_{i4l2} & 0 & \sum_{i=1}^{N}\sum_{l=1}^{N} L_{i4l4} \end{bmatrix} \tag{16}$$

The diagonal terms in the above matrix are the sectional partial self-inductance and the off-diagonal terms are the sectional partial mutual inductance. Note that the signs of sectional self-inductance are positive and sectional partial mutual inductance are negative for rectangular structures. The summation terms can be evaluated by calculating some general matrices like L_{N1k1}, L_{N1k3}. The inductance contributions of L_{N2k2}, L_{N2k4} can be obtained by inverting $a \leftrightarrow b$ in the previous set of general expressions. The net self-inductance can then be written as

$$L = \sum_{i=1}^{N}\sum_{j=1}^{4}\sum_{l=1}^{N}\sum_{k=1}^{4} L_{ijlk} \tag{17}$$

3.1. Sectional Partial Inductances

The sectional partial self-inductance is defined as the sum of the partial self and partial mutual inductance contributions of current in a particular section on the same section on all possible turns. The sectional partial mutual self-inductance is defined as the sum of the partial mutual inductance contributions of current in a particular section on a different section for all combinations of possible turns. Following the previous procedures, the partial self-inductance due to current in the N^{th} turn first section on the k^{th} turn first section is given by

$$L_{N1k1} = \frac{\mu_0}{4\pi} \times \left[\int_{k_1}^{k_2} dx_1 \int_{\alpha}^{\beta} \frac{dx_2}{\sqrt{(x_2 - x_1)^2 + \left(r + (N-k)(2r + l_g)\right)^2}} \right]$$

Symbols:

$$k_1 = \left(-\frac{a}{2} + r\right) - (k-1)(2r + l_g),\ k_2 = \left(\frac{a}{2} - r\right) + (k-1)(2r + l_g)$$

$$\alpha = -\frac{a}{2} - (N-1)(2r + l_g),\ \beta = \frac{a}{2} + (N-1)(2r + l_g) \tag{18}$$

The result of this integration is the same as (14) with $I(C)$ defined as

$$\begin{aligned} I(C) = &\sqrt{\left(r + (N-k)(2r + l_g)\right)^2 + (C - k_2)^2} \\ &- \sqrt{\left(r + (N-k)(2r + l_g)\right)^2 + (C - k_1)^2} \\ &+ \ln \left| \frac{\left(\sqrt{\left(r + (N-k)(2r + l_g)\right)^2 + (C - k_1)^2} + (C - k_1) \right)^{(C-k_1)}}{\left(\sqrt{\left(r + (N-k)(2r + l_g)\right)^2 + (C - k_2)^2} + (C - k_2) \right)^{(C-k_2)}} \right| \end{aligned} \tag{19}$$

Similarly, the partial mutual self-inductance can be written as

Preprints (www.preprints.org) | NOT PEER-REVIEWED | Posted: 26 May 2017 doi:10.20944/preprints201705.0191.v1

Peer-reviewed version available at Energies 2017, 10, , 774; doi:10.3390/en10060774

$$L_{N1k3} = \frac{\mu_0}{4\pi} \times \left[\int_{k_1}^{k_2} dx_1 \int_{\alpha}^{\beta} \frac{dx_2}{\sqrt{(x_2 - x_1)^2 + \left((b-r) + (2r+l_g)(N+k-2)\right)^2}} \right] \tag{20}$$

Symbols:

$$k_1 = \left(-\frac{a}{2} + r\right) - (k-1)(2r+l_g), k_2 = \left(\frac{a}{2} - r\right) + (k-1)(2r+l_g)$$
$$\alpha = -\frac{a}{2} - (N-1)(2r+l_g), \beta = \frac{a}{2} + (N-1)(2r+l_g)$$

Again, the result of this integration is the same as (14) with $I(C)$ defined as

$$\begin{aligned} I(C) = &\sqrt{((N+k-2)(2r+l_g) + (b-r))^2 + (C-k_2)^2} \\ &-\sqrt{((N+k-2)(2r+l_g) + (b-r))^2 + (C-k_1)^2} \\ &+ \ln \left| \frac{\left(\sqrt{((N+k-2)(2r+l_g) + (b-r))^2 + (C-k_1)^2} + (C-k_1)\right)^{(C-k_1)}}{\left(\sqrt{((N+k-2)(2r+l_g) + (b-r))^2 + (C-k_2)^2} + (C-k_2)\right)^{(C-k_2)}} \right| \end{aligned} \tag{21}$$

4. Mutual Inductance between rectangular coils

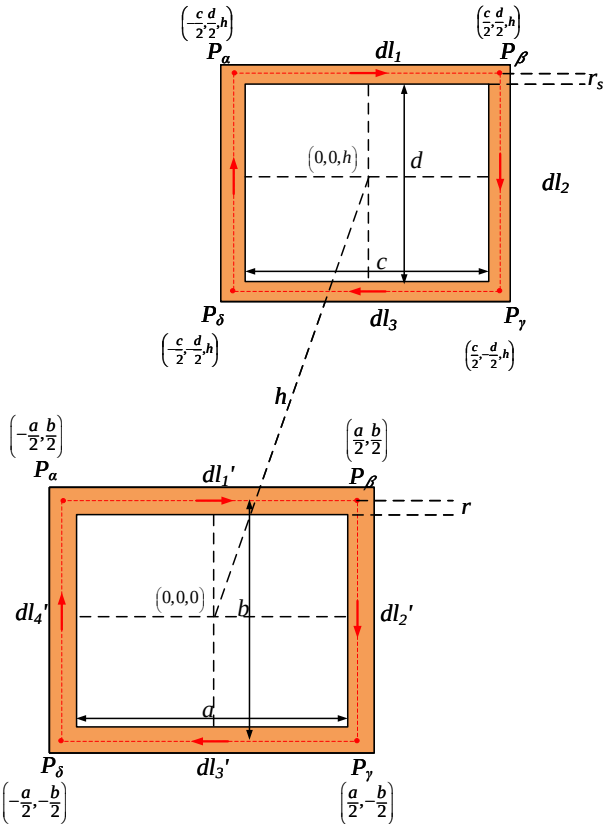

Figure 4. Mutual inductance between a general single turn primary and a single turn secondary. The length and breadth of the primary are (a, b) while that of the secondary are (c, d). The vertical displacement between the primary and secondary is h.

A simple description of the mutual inductance scenario of a single turn primary and a single turn secondary is depicted in Figure 4. As an extension of the theory previously developed, the mutual inductance for a multi-turn rectangular coil can be written in terms of the contributions due to current flowing through i^{th} turn, j^{th} section of the primary on the l^{th} turn, k^{th} section on the secondary. The sectional mutual inductance matrix can be written as

$$M_{ijlk} = \frac{\mu_0}{4\pi} \times \begin{bmatrix} \sum_{i=1}^{N}\sum_{l=1}^{N} M_{i1l1} & 0 & -\sum_{i=1}^{N}\sum_{l=1}^{N} M_{i1l3} & 0 \\ 0 & \sum_{i=1}^{N}\sum_{l=1}^{N} M_{i2l2} & 0 & -\sum_{i=1}^{N}\sum_{l=1}^{N} M_{i2l4} \\ -\sum_{i=1}^{N}\sum_{l=1}^{N} M_{i3l1} & 0 & \sum_{i=1}^{N}\sum_{l=1}^{N} M_{i3l3} & 0 \\ 0 & -\sum_{i=1}^{N}\sum_{l=1}^{N} M_{i4l2} & 0 & \sum_{i=1}^{N}\sum_{l=1}^{N} M_{i4l4} \end{bmatrix} \tag{22}$$

5. Extension to MCCP

Consider a linear magnetic system excited by a pure sinusoidal (non-harmonic) voltage consisting of a primary and pickup composed of several segmented coils as shown in Figure 5. The coils can be individually connected serially or in parallel to compose the multi-coil charge-pad. Let the primary be composed of $'n'$ coils, $(1, 2, ..n)$ and pickup with $'m - n'$ coils, $(n+1, n+2, ..m, (m > n))$. Consequently, the voltage matrix, $\left[V\right]$ for all the coils can be written as a in terms of currents, $\left[i\right]$ and time-derivative of currents, $\left[\frac{di}{dt}\right]$

$$\left[V\right] = \left[L\right] \times \left[\frac{di}{dt}\right] + \left[R\right] \times \left[i\right] \tag{23}$$

Where the matrices are defined as

$$[V] = \begin{bmatrix} v_1 \\ v_2 \\ \vdots \\ v_n \\ v_{n+1} \\ v_{n+2} \\ \vdots \\ v_m \end{bmatrix} \left[\frac{di}{dt}\right] = [i'] = \begin{bmatrix} i'_1 \\ i'_2 \\ \vdots \\ i'_n \\ i'_{n+1} \\ i'_{n+2} \\ \vdots \\ i'_m \end{bmatrix} [i] = \begin{bmatrix} i_1 \\ i_2 \\ \vdots \\ i_n \\ i_{n+1} \\ i_{n+2} \\ \vdots \\ i_m \end{bmatrix} [R] = \begin{bmatrix} R_1 & 0 & 0 & 0 & 0 & 0 & 0 & 0 \\ 0 & R_2 & 0 & 0 & 0 & 0 & 0 & 0 \\ \vdots & \vdots & \vdots & \vdots & \vdots & \vdots & \vdots & \vdots \\ 0 & 0 & 0 & 0 & 0 & 0 & 0 & R_8 \end{bmatrix} \tag{24}$$

Preprints (www.preprints.org) | NOT PEER-REVIEWED | Posted: 26 May 2017 doi:10.20944/preprints201705.0191.v1

Peer-reviewed version available at Energies 2017, 10, , 774; doi:10.3390/en10060774

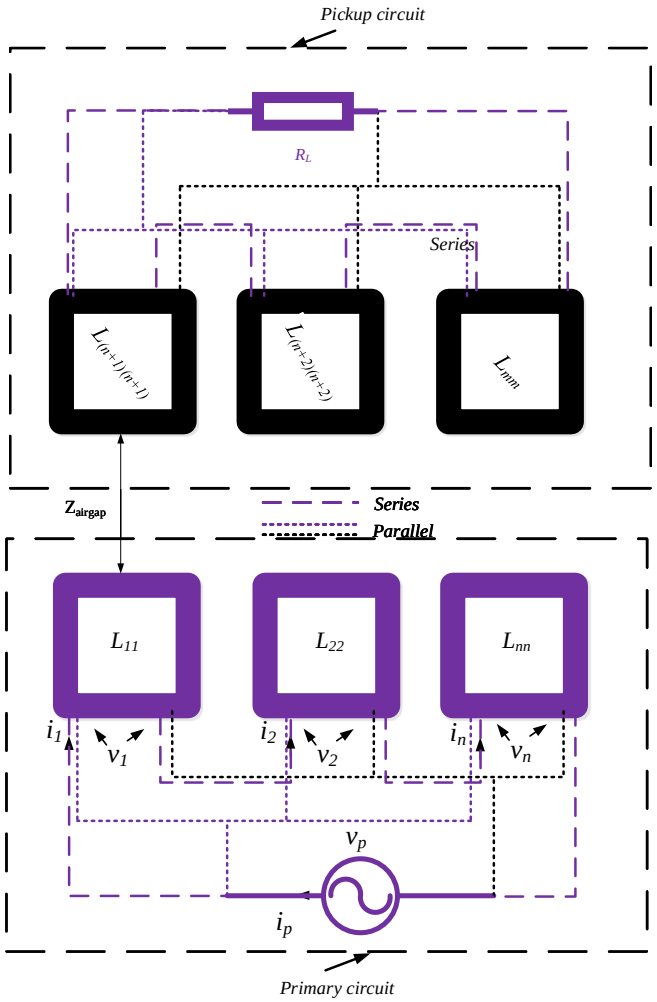

Figure 5. Defining a IPT system with primary and secondary composed of multiple coils with self-inductances as $(L_{ij}, i = j)$ and mutual inductances as $(L_{ij}, i \neq j)$.

Finally, $[L]$ is defined as

$$[L] = \begin{bmatrix} L_{11} & L_{12} & \dots & L_{1n} & L_{1(n+1)} & L_{1(n+2)} & \dots & L_{1(m)} \\ L_{21} & L_{22} & \dots & L_{2n} & L_{2(n+1)} & L_{2(n+2)} & \dots & L_{2(m)} \\ \vdots & \vdots & \vdots & \vdots & \vdots & \vdots & \vdots & \vdots \\ L_{n1} & L_{n2} & \dots & L_{nn} & L_{n(n+1)} & L_{n(n+2)} & \dots & L_{n(m)} \\ L_{(n+1)1} & L_{(n+1)2} & \dots & L_{(n+1)n} & 0 & 0 & 0 & 0 \\ L_{(n+2)1} & L_{(n+2)2} & \dots & L_{(n+2)n} & 0 & 0 & 0 & 0 \\ \vdots & \vdots & \vdots & \vdots & 0 & 0 & 0 & 0 \\ L_{m1} & L_{m2} & \dots & L_{mn} & 0 & 0 & 0 & 0 \end{bmatrix} \quad (25)$$

The series and parallel combination can now be decomposed from this multi-coil combination. In case of a series connected set of coils, $i_p = i_1 = i_2 \cdots = i_n$ and $i_s = i_{n+1} = i_{n+2} \cdots = i_m$. Also, in case of the parallel set of coils, $i_p = i_1 + i_2 \cdots + i_n$ and $i_s = i_{n+1} + i_{n+2} \cdots + i_m$. After such a transformation, it becomes easy to reduce such a system of parallel or series coils into a single coil-pair. In such a system, for both series and parallel system of coils, it can be easy to prove that

Preprints (www.preprints.org) | NOT PEER-REVIEWED | Posted: 26 May 2017 doi:10.20944/preprints201705.0191.v1

Peer-reviewed version available at Energies 2017, 10, , 774; doi:10.3390/en10060774

$$\begin{bmatrix} \sum_{i=1}^{n} v_i \\ \sum_{j=n+1}^{m} v_j \end{bmatrix} = \begin{bmatrix} \sum_{i=1}^{n}\sum_{j=1}^{n} L_{ij} & \sum_{i=1}^{n}\sum_{j=n+1}^{m} L_{ij} \\ \sum_{j=n+1}^{m}\sum_{i=1}^{n} L_{ij} & \sum_{j=n+1}^{m}\sum_{i=n+1}^{m} L_{ij} \end{bmatrix} \times \begin{bmatrix} i_p' \\ i_s' \end{bmatrix} + \begin{bmatrix} \sum_{i=1}^{n} R_i & 0 \\ 0 & \sum_{j=n+1}^{m} R_j \end{bmatrix} \times \begin{bmatrix} i_p \\ i_s \end{bmatrix} \quad (26)$$

The Equation (26) indicates that it is possible to convert a linear magnetic system with multi-coil

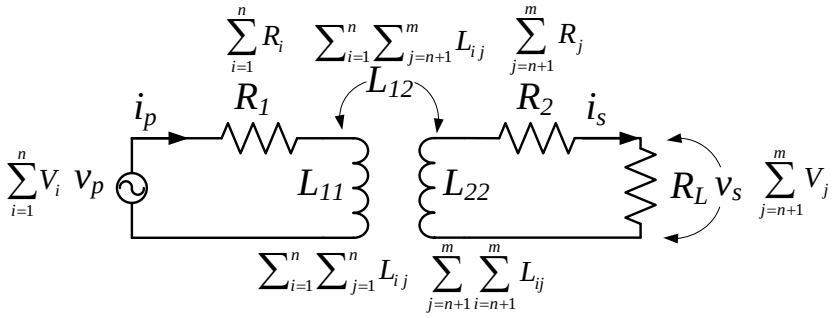

Figure 6. Equivalent single coil pair for a system of coils with $(1, 2..n)$ coils in the primary and $(n+1, n+2..m)$ coils in the pickup.

into a system of a single coil pair by calculating the individual contributions. Such a equivalent coil system is shown in Figure 6. Such a transposition makes it easy to analytically model multi-coil linear magnetic systems by using the principles of single coils already developed previously.

6. Validation of Analytical Model

To validate the analytical models that are developed in previous sections, FEM simulation and experimentation are carried out. Circular and rectangular shapes are compared. The physical properties of the coils are tabulated in Table 1. To show the efficacy of analytical expressions, a reduced fill factor was employed for rectangular coils by maintaining an air-gap of 0.6 cm between the turns.

Table 1. Properties of the compared circular and rectangular coils

Type of coil	a (cm)	b (cm)	l_g (cm)	N (turns)
Rectangular $(R1)$	4	2	0.6	9
Rectangular $(R2)$	6	4	0.6	15
Circular (C)	inner diameter = 5.5 cm			14
litz wire used	600×0.071 mm, 2.1 mm dia overall			

The constructed coils are shown in Figure 7. The measurements, analysis and simulations are carried out at variable z-gaps between the coils and also at several misaligned positions. The z-gaps are simulated at 3, 5, 7 and 9 cms of coil displacements in the z-direction, taking vertical misalignment in consideration. In case of lateral misalignment, perfect alignment, 75%, 50% and 25% alignments are chosen along x-axis. The results along y-axis for symmetrical shapes follows the same trend as the x-axis and hence are not considered.

Measurements are made by using Agilent 4294A impedance analyser. The mutual inductances are extracted from self-inductances by carrying out a constructive and destructive flux measurement

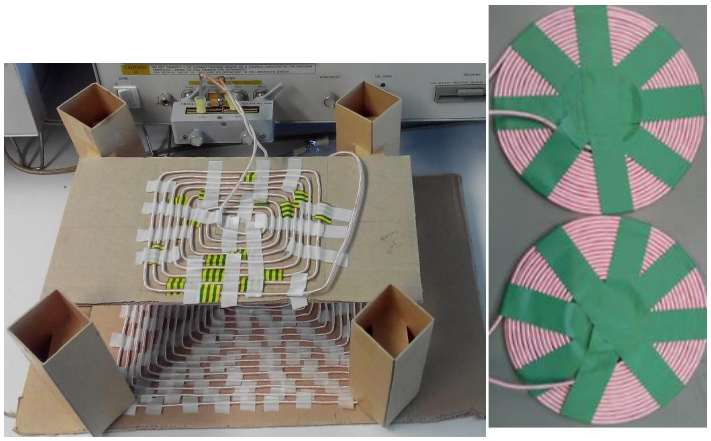

Figure 7. Experimental comparison of rectangular and circular coils with parameters as tabulated in Table 1.

by connecting the coils serially from one end to the other and then swapping one of the ends (L_{const}, L_{des}). The expressions used for extracting the mutual inductance and coupling are

$$M = \frac{L_{const} - L_{des}}{4}$$
$$k = \frac{M}{\sqrt{L_1 L_2}} \tag{27}$$

The analytical expressions for circular coils are calculated from Equations (1) − (4). Also, for rectangular coils, Equations (12) − (22) are computed. MATLAB scripts are written separately for each of the computation and a software tool for self, mutual and coupling computations is developed for air-cored coils. A comparison of coupling obtained analytically and by making measurements for circular coils is presented in Figure 8.

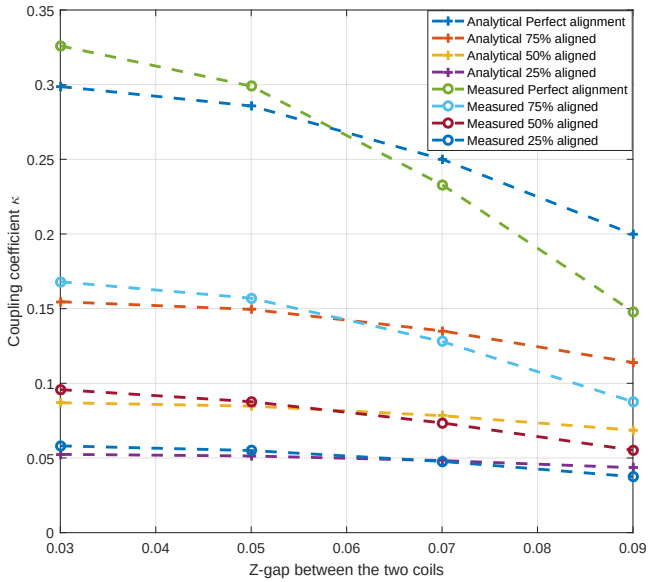

Figure 8. The analytical and experimental comparison of coupling coefficient of circular coils with Z-gaps of 3, 5,7 and 9 cms with coils of parameters as tabulated in Table 1.

Preprints (www.preprints.org) | NOT PEER-REVIEWED | Posted: 26 May 2017 doi:10.20944/preprints201705.0191.v1

Peer-reviewed version available at Energies 2017, 10, , 774; doi:10.3390/en10060774

The results show a large degree of agreement between the analytical expressions and the measured results. Mismatch in the results are due to the use of litz wire in the experiments (unlike a solid conductor used in the analysis) and eddy currents (proximity effects) in the coils that are not considered in the analytical expressions. Some instrumental accuracy limitations also add to this error. However, most observations are within 1% accuracy except for an odd set in the neighbourhood of 6%. These accuracy measures are acceptable for magnetic analysis.

FEM models were created and simulated so as to perform numerical evaluation of the coils considered. The FEM models developed are presented in Figure 9.

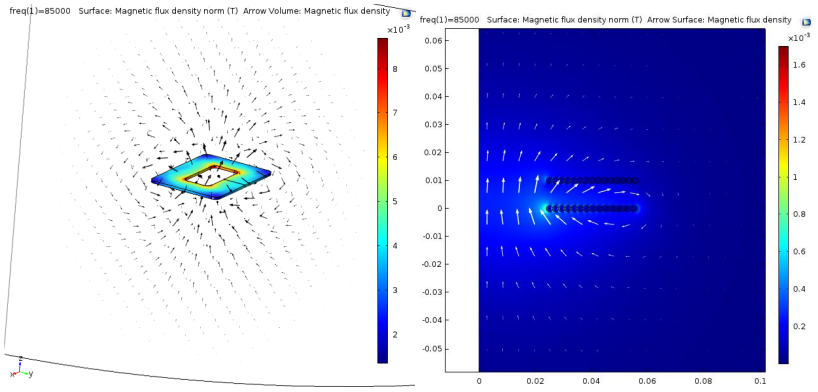

Figure 9. FEM simulation models of the rectangular coil (top-left), circular coil (top-right) and the rectangular coil (bottom) couple. The rectangular coils are modelled in a 3d domain while the circular coils due to their rotational symmetry are modelled in the 2d domain.

The coupling and self-inductances of circular and rectangular coils are compared analytically, using FEM simulations and experimentation. The results are presented in Figure 10, the coupling being recorded at perfect alignment and variable z-gaps while self-inductances measured for all variable shapes. All measurements show the same trend and there is a close match between analytical observations, FEM simulations and measurements.

Figure 10. Coupling coefficient and self-inductances of air-cored charge pads of various shapes. The coupling is measured at various z-gaps at the best aligned point. The parameters of the coils are as presented in Table 1.

7. Shape and Performance of Air Couplers

The effect of shapes in IPT systems can be analysed for air-cored couplers based on the mathematical analysis that has been derived previously. To make such a comparison, a few performance parameters are considered. They are the open circuit voltage v_{oc}, short circuit current i_{sc}, maximum output power, s_{max} and maximum efficiency, η_{max}. Open circuit voltage is the maximum voltage that the IPT system can source and short circuit current is the maximum current that the same can deliver.

For a coupled charge-pad, if L_1 and L_2 are the self-inductances of the two couplers with 'M' as the mutual inductance and operated at angular frequency ω, creating current i_1 through the primary, the open-circuit voltage is defined as $v_{oc} = j\omega M i_1$ and during short-circuit if i_{sc} is the current flowing in the pickup, $i_{sc} = \frac{v_{oc}}{j\omega L_2} = \frac{M i_1}{L_2}$. Now, the maximum output power is defined in terms of loaded quality factor of pickup, $Q_{2L} = (\omega \times L_2)/(R_L + R_2)$, where R_L is the load resistance and R_2 is the ac-resistance of the pickup charge-pad as

$$s_{max} = v_{oc} \times i_{sc} = \frac{(i_1^2 M^2 Q_{(2,L)} \omega)}{L_2} \tag{28}$$

The above equation quantifies the maximum output power that such an air-cored coupler can source. Also, the maximum efficiency of IPT systems have been derived independent of compensation applied and load present in terms of native quality factors of the primary (Q_1) and pickup (Q_2) as [13]

$$\eta_{max} = \frac{k\sqrt{Q_1 Q_2}}{2 + k\sqrt{Q_1 Q_2}} \tag{29}$$

These parameters have been used to compare a number of differently shaped air-cored charge-pads. All shapes considered have been analysed keeping area conserved. This way, generalizations of the behaviour of fields and hence coupling, power transferred and other parameters are possible. Several analysis were also carried out keeping perimeter conserved and multi-turns with similar results. In addition, these results also correspond and can be generalized to charge-pads with flux-enhancing materials such as ferrite. This as enhanced coupling is obtained by placing ferrites along the natural direction of flux lines. Hence, the basic tendency of the shape in terms of coupling and its gradient is similar in all IPT applications. The compared shapes are listed in Table 2. All considered shapes have been simulated with a one turn coil and a z-gap of 1 cm. This so that the effect of shapes are more enhanced.

Table 2. Physical parameters of various coil shapes used in the air-cored coupler.

Considered Shape	Parameters
Rectangle dim.(mm)	650×400
Square dim.(mm)	509.9×509.9
Circle rad.(mm)	287.6
Double Circle (DC) dim.(mm)	203.4
Double Rectangle (DR) symmetric dim.(mm)	459.6×282.8
Double Rectangle + Quadrature symmetric dim.(mm) (DR+Q)	375.3×230.9
Area (m^2)	0.2600

The multi-coil shapes are composed of multiple symmetric coils that are placed close to each other with the coils carrying currents in opposite direction. The mutual inductance and coupling of these charge-pads are obtained by analysing (26) and using the mathematical analysis of single coils.

A study of coupling by misaligning the coils along x-direction (lateral displacement) is presented in Figure 11.

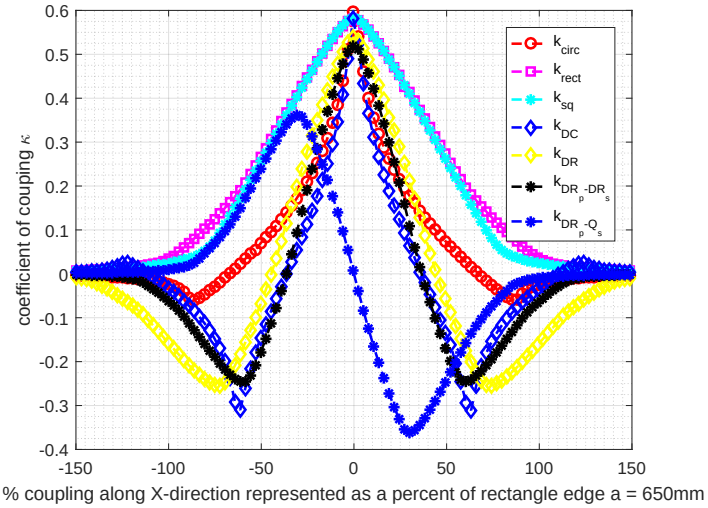

Figure 11. Coupling coefficients of single and multi-coil shapes with x-directional misalignment of coils in Table 2.

It can be inferred that circle and four sided shapes differ in the tolerance to coupling variations when subjected to lateral misalignment. The coupling of rectangular and square coils tend to decay gradually, while the circular shape sees a more sharper drop with misalignment. Circular shape due to the fact that it has the highest area for a given perimeter among closed shapes, has the highest coupling at the best aligned point. The double coils also share the same feature but with a larger extension of the power profile. It is important to note that in this analysis, since area is kept conserved, the perimeter varies between the shapes and hence it is important to keep trends in mind, rather than absolute values. Null-coupling points in DR and DC coils, occur at positions where a pick-up coil is confronted with opposing flux of equal magnitude from the primary charge-pad. Among the double coils, the DC geometry has greater best-aligned coupling than that of DR geometry. However, the misalignment profile for DR coils is broader than that of DC coils and hence it is well suited to applications where larger misalignment behaviour is expected, for eg: EVs. When such an analysis was broadened to include the behaviour of a DR primary and a DRQ pick-up, the Q picking up flux emanating from a DR primary behaves best at the misaligned points, while is the worst at the best-aligned point. On the contrary, the DR pick-up behaves complementary to the Q pick-up with a DR primary.

Power transferred to the pick-up is evaluated from Equation (28). The uncompensated power calculated when subjected to lateral misalignment is shown in Figure 12. Among single coils, the circular coil has a sharp misalignment band while the four sided shapes have greater tolerance. The double shapes follow the features of their single equivalents, with the difference that there is a misalignment point when a single coil among both the primary and pick-up receives power. This creates two more zones of power transfer apart from the best aligned point. In these points, the power is reduced to $< 25\%$ as the pick-up voltage is reduced to half, which in turn halves the pick-up current. However, these double shapes suffer from a no-power zone created at the null coupling points. These null power points can be eliminated by using a quadrature coil, the coupling of which is complementary to the main coils and hence an addition of power from the quadrature coils removes these null zones. It is important to note that in an actual implementation, the magnitudes of these curves will depend on the number of turns of each coil, materials present, the source characteristic - voltage/current, resonant behaviour etc.

Preprints (www.preprints.org) | NOT PEER-REVIEWED | Posted: 26 May 2017 doi:10.20944/preprints201705.0191.v1

Peer-reviewed version available at Energies 2017, 10, , 774; doi:10.3390/en10060774

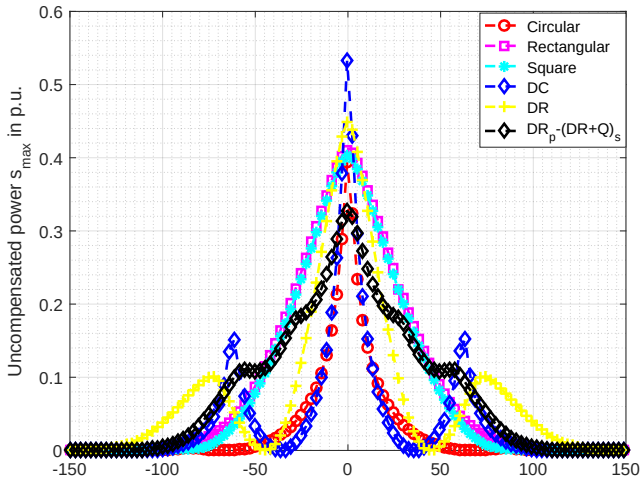

Figure 12. Uncompensated power analysed on the basis of a unit current flowing through various shapes of single turn and equal area as indicated in Table 2. The misalignment is considered along x-direction.

The maximum efficiency as presented in Equation (29) has dependence on quality factor which in-turn depend on the ac resistances of the coils. The ac-resistances for the *litz* wire used is extracted from a tabulation technique as presented in [14]. The calculated ac resistance factor including both skin and proximity effects for litz wire indicated in Table 1 is $\frac{R_{ac}}{R_{dc}} = 1.029$. The result of maximum efficiency computation when subjected to variable coupling during misalignment is shown in Figure 13. This plot represents the theoretical maximum efficiency that can be expected at various misaligned points for various shapes. The efficiency values floor at the power null points as expected.

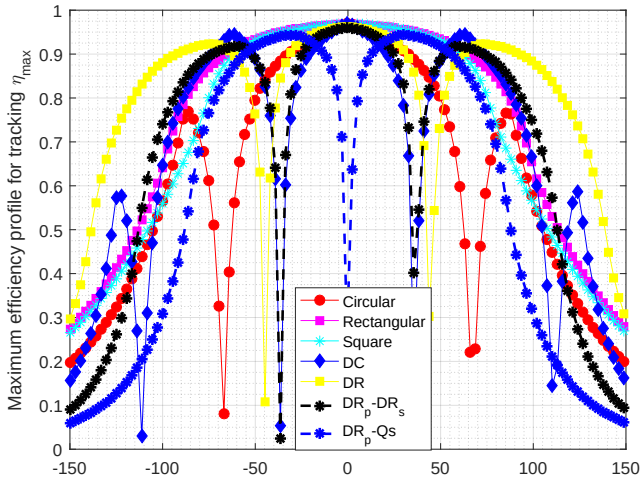

Figure 13. Maximum efficiency profile tracking with x-directional misalignment of coils in Table 2.

8. Discussion

In this paper, a generic analytical tool that is useful to model the magnetics of single and multi coil geometries is developed. The analytical equations developed can be extended to polygonal shapes and can be used to model n-multi coil geometries as well. This is a first step in magnetic design, wherein the fundamental magnetics can be evaluated. A detailed numerical optimization based on the inputs from this study so as to optimize ferrite, aluminium and other materials that may

be present in charge-pads is the next step. Such a FEM optimisation for a 1kW DR system is presented in [15]. Some useful results obtained from the analysis are:

1. The analysis, compared with FEM and experiments have a good match. Almost all observations have an error less than 10%. This is acceptable for magnetic analysis.
2. The coupling of single coils are such that circular coils have the best coupling at the well-aligned point and the four shaped coils have a larger misalignment tolerant band. Thus, rectangular coils can be used for more misalignment tolerant designs and circular for well-aligned applications.
3. The coupling behaviour of multi-coil geometries follow the trend of single-coil shapes but have null-coupling points. By designing a Q coil located between the mid points of the single-coils, flux can be captured at the null-coupling points.
4. The Q and DR pickup have complementary coupling-misalignment behaviour. At the best aligned point, the Q picks up no flux and at the misalignment point of null-coupling of DD pickup, the Q picks up maximum flux.
5. The DR and DC shapes can effectively extend the range of power transfer to larger misaligned positions. The addition of Q to the pickup can remove null-coupling points from the power profile.
6. Rectangular coils also perform well with the same enclosed area as multi-coil geometries, with a lesser zone of power transfer.
7. The total enclosed area of the shapes has been kept constant to make a fair comparison. However, it is possible to influence the turns in the Q coils in DRQ and this impacts the peaks obtained in the misalignment points. For designing IPT systems that are adapted to misalignment as in EVs during motion, dynamic power transfer, a DR charge pad on the roadway would be a good solution optimizing the excess material costs involved in building DRQ pads. Also, EVs travelling along the regions of power null for a long time is limited. However, for stationary charging, misalignment tolerant DRQ charge pad for both primary and secondary is a good choice for good power transfer. Also, interoperability is possible between these pads thus making it possible to have the same vehicle pads for both modes of operation.

Author Contributions: "V.P. is the primary investigator. S.B. made several numerical models to evaluate the theory developed. P.B. and J.A.F. are the supervisors who directed the study and gave valuable suggestions and shared their experiences in this field."

Conflicts of Interest: "The authors declare no conflict of interest."

References

1. Prasanth, V.; Bauer, P.; Ferreira, J.A. A sectional matrix method for IPT coil shape optimization. In International Conference on Power Electronics and ECCE Asia (ICPE-ECCE Asia), Daejeon, Korea, 5–6 June 2015, pp. 1684–1691.
2. Prasanth, V.; Bandyopadhyay, S.; Bauer, P.; Ferreira, J.A. Analysis and comparison of multi-coil inductive power transfer systems. In Power Electronics and Motion Control Conference (PEMC), 2016 IEEE International , Varna, Bulgaria, 25–30 Sept 2016, pp. 993–999.
3. Covic, G.A.; Boys, J.T. Modern Trends in Inductive Power Transfer for Transportation Applications. *IEEE Trans. Emerg. Sel. Topics Power Electron.* **2013**, *1*, 28–41.
4. Prasanth, V.; Bauer, P. Distributed IPT Systems for Dynamic Powering: Misalignment Analysis. *IEEE Trans. Ind. Electron.* **2014**, *61*, 6013–6021.
5. Shekhar, A.; Prasanth, V.; Bauer, P; Bolech, M. Economic Viability Study of an On-Road Wireless Charging System with a Generic Driving Range Estimation Method. *Energies* **2016**, *9*, 76.
6. Budhia, M.; Covic, G.A.; Boys, J.T. Design and optimization of circular magnetic structures for lumped inductive power transfer systems. *IEEE Trans. Power Electron.* **2011**, *26*, 3096–3108.
7. Shin, J.; Shin, S.; Kim, Y.; Ahn, S.; Lee, S.; Jung, G.; Jeon, S.-J.; Cho, D.-H. Design and Implementation of Shaped Magnetic-Resonance-Based Wireless Power Transfer System for Roadway-Powered Moving Electric Vehicles. *IEEE Trans. Ind. Electron.* **2014**, *61*, 1179–1192.

8. Grover, F.W.; In *Inductance Calculations: Working Formulas and Tables*; Dover Publications, 1946.
9. Convway, J.T. Inductance calculations for noncoaxial coils using bessel functions. *IEEE Trans. Mag.* **2007**, *43*, 1023–1034.
10. Maxwell, J.C.; In *A Treatise on Electricity and Magnetism*; Cambridge University Press: Cambridge, UK, 2010.
11. Ruehli, A.; Paul, C.; Garrett, J. In Proceedings of International Symposium on Electromagnetic Compatibility, 1995 pp. 7–12.
12. Musing, A.; Ekman, J.; Kolar, J.W. Efficient calculation of non-orthogonal partial elements for the peec method. *IEEE Trans. Mag.* **2009**, *45*, 1140–1143.
13. Takanashi, H.; Sato, Y.; Kaneko, Y.; Abe, S; Yasuda, T. A large airgap 3kw wireless power transfer system for electric vehicles. In Energy Conversion Congress and Exposition (ECCE) , 2012 IEEE, pp. 269–274.
14. Terman, F.E.; In *Radio Engineer's Handbook*; 1943.
15. Bandyopadhyay, S.; Prasanth, V.; Bauer, P.; Ferreira, J.A. Multi-Objective Optimisation of Distributed IPT Systmes for charging of Electric Vehicles . In IEEE Transportation Electrification Conference and Expo (ITEC), 2016 IEEE International , Detroit, US.